Nisula, Mikko; Karttunen, Antti J.; Solano, Eduardo; Tewari, Girish C.; Karppinen, Maarit; Minjauw, Matthias; Jena, Himanshu Sekhar; Van Der Voort, Pascal; Poelman, Dirk; Detavernier, Christophe

Emergence of Metallic Conductivity in Ordered One-Dimensional Coordination Polymer Thin Films upon Reductive Doping

Published in:
ACS Applied Materials and Interfaces

DOI:
10.1021/acsami.1c01738

Published: 03/03/2021

Document Version
Peer-reviewed accepted author manuscript, also known as Final accepted manuscript or Post-print

Emergence of metallic conductivity in ordered 1D coordination polymer thin films upon reductive doping

Mikko Nisula[1*], Antti J. Karttunen[2], Eduardo Solano[3], Girish C. Tewari[2], Maarit Karppinen[2], Matthias Minjauw[1], Himanshu Sekhar Jena[4], Pascal Van Der Voort[4], Dirk Poelman[1], Christophe Detavernier[1*]

1. Department of Solid State Sciences, Ghent University, B-9000, Ghent Belgium

2. Department of Chemistry and Materials Sciences, Aalto University, FI-00076, Espoo, Finland

3. NCD-SWEET Beamline, ALBA Synchrotron Light Source, 08290 Cerdanyola del Vallès, Spain

4. Department of Chemistry, Ghent University, B-9000, Ghent, Belgium

*Corresponding authors: mikko.nisula@ugent.be; christophe.detavernier@ugent.be

Abstract:

The prospect of introducing tuneable electric conductivity in metal-organic coordination polymers is of high interest for nanoelectronic applications. As the electronic properties of these materials are strongly dependent on their microstructure, the assembly of coordination polymers into thin films with well-controlled growth direction and thickness is crucial for practical devices. Here, we report the deposition of 1D coordination polymer thin films of N,N'-dimethyl dithiooxamidato-copper by atomic/molecular layer deposition. High out-of-plane ordering is observed in the resultant thin films suggesting the formation of a well-ordered secondary structure by the parallel alignment of the 1D polymer chains. We show that the electrical conductivity of the thin films is highly dependent on their oxidation state. The as-deposited films are nearly insulating with electrical conductivity below 10^{-10} S/cm with semiconductor-like temperature dependency. Partial reduction with H_2 at elevated temperature leads to an increase in the electrical conductivity by 8 orders of magnitude. In the high-conductance state, metallic behaviour is observed over the temperature range of 2 – 300 K. Density functional theory calculations indicate that the metallic behaviour originates from the formation of a half-filled energy band intersecting the Fermi level with the conduction pathway formed by Cu-S-Cu interaction between neighbouring polymer chains.

Introduction:

Coordination polymers are a class of hybrid materials in which coordination compounds of a metal centre and interlinking ligands form extended repeating structures. Their attractiveness arises from the synthetic tuneability of their physical and chemical properties with almost limitless selection of the

metal and ligand combinations. For instance, electrical conductivity in coordination polymers can be achieved from suitable overlap of frontier orbitals of the constituent metal centre and the organic ligands.[1] New two-dimensional materials akin to graphene could be obtained from synthesising sheet-like d-π conjugated coordination polymers, whereas conductive 1D-polymers can take the role of molecular wires.[2] In this way, electrically conductive materials with tuneable properties would help pushing the down-sizing limit of nanoelectronic devices into the molecular dimensions.[3]

However, the prime limiting factor in utilizing coordination polymers for devices is their poor processability. Typical precipitation-based synthesis routes yield nano/micron sized crystallites that are very difficult to further process into high-quality thin films required for applications.[4] Furthermore, also the electronic properties are crucially dependent on the quality of the synthesis product. In recent years highly conductive 2D layered coordination polymers have been reported.[5–9] Computational studies predict metallic conductivity for several of these materials, but the experimental results almost invariably show a thermally activated conduction mode indicative of the presence of a band gap.[10–13] So far, only in few cases, clear metallic behaviour has been observed in conductance measurements.[8,14,15] In 1D linear-backbone polymers, metallic conductivity has been observed for instance in halogen-bridged MMX chains where the metallic behaviour stems from hybridization of the metal and halogen orbitals leading to formation of a half-filled band at the Fermi-level.[16–19] Also, a suitable metal-metal interaction can promote metallic conduction.[20] However, delocalization over the organic ligand has only been theoretically predicted with indirect experimental evidence of metallic behaviour.[21,22] It is apparent that the discrepancy for both 1D and 2D materials arises from defects and grain boundaries that dominate the conductance.[5,23–25]

Therefore, robust synthetic routes for thin films with high degree of ordering and well-controlled thickness are needed not only for practical applications but also for fundamental understanding of transport phenomena of conductive coordination polymers. Here, we demonstrate that the emerging atomic/molecular layer deposition (ALD/MLD) technique is well-suited for this task. MLD is a vapour phase deposition technique closely related to the better-known Atomic Layer Deposition (ALD). Both techniques are defined by the sequential, self-saturating exposure of vapour-phase precursors onto surfaces. This monolayer accuracy in process control leads to sub-nanometre level precision in layer thickness control and excellent uniformity over large area substrates, as well as over high-aspect ratio structures. While ALD involves inorganic compounds only, MLD expands the same self-limiting gas-surface reaction approach to the polymeric materials with the implementation of volatile organic molecules as precursors.[26] By alternating the metal and organic reactants, this gas-phase layer-by-layer approach leads to the controlled synthesis of ultra-high-quality coordination polymer thin films. An added benefit is that the often-unwanted inclusion of solvent molecules in the product is naturally

avoided.[27–29] Recent advances in the ALD/MLD approach have enabled the fabrication of several new crystalline coordination network thin films.[30–33]

Here we target the deposition of 1D dimethyl dithiooxamidato-copper (hereafter Cu-DMD, see also Figure 1a) thin films. These films display long-range ordering with high out-of-plane orientation as determined by grazing-incidence wide angle X-ray scattering (GIWAXS). In the as deposited (oxidized) state the films show very low conductance of $< 10^{-10}$ S cm^{-1}. However, upon reduction induced by annealing in hydrogen containing atmosphere, the conductance can be continuously increased over 8 orders of magnitude up to 10^{-2} S cm^{-1}. In the high conductance state, the films display metallic behaviour in the temperature range of 2 – 300 K. Complementary density functional theory calculations predict that the metallic behaviour arises from the formation of a half-filled electron band intersecting the Fermi level upon reduction.

Experimental section:

The samples were deposited using a home-built pump-type high-vacuum ALD reactor with a base pressure of 10^{-5} mbar. The sample temperature during the deposition was 80 °C, whereas the reactor chamber walls were heated to 85 °C. Bis(dimethylamino-2-propoxy)copper(II) (Cu(dmap)2, >97 %, Strem Chemicals) and N,N'-dimethyldithiooxamide (DMD) were used as the precursors. The N,N'-dimethyldithiooxamide was synthesized following previously a reported synthesis route.[34] In short 5 g of dithiooxamide (97 %, Sigma Aldrich) was mixed with 3 times molar excess of aqueous methylamine (40 % wt. in H_2O, Sigma Aldrich) under constant stirring. When heated to 40 °C, a bright yellow precipitate was observed to form within 30 minutes. The precipitate was filtered and washed several times with H_2O. 1H NMR (CDCl3; 300 MHz): 10.29 (2H, b, NH), 3.23 (6H, d, J = 3, CH3)

For the sample deposition, $Cu(dmap)_2$ and DMD were delivered from bubblers heated to 70 °C and 60 °C, respectively, with argon as a carrier gas for delivery to the reactor chamber. For the precursor pulses, a stop-flow method was used, whereby the reactor chamber pressure was increased to ~1 mbar with the precursor/argon mixture and then left to react for the duration of the pulse. After each pulse, the chamber was pumped back to the base pressure before the introduction of the next precursor pulse. Unless otherwise mentioned, all samples were deposited on 3 cm x 3 cm Si(100) substrates with native oxide.

The film growth was studied *in-situ* by spectroscopic ellipsometry (SE). The thickness was obtained by fitting the recorded data using a General Oscillator model in the CompleteEase software package. The ellipsometer used was a J.A. Woollam M-2000 with a wavelength range of 245 nm to 1500 nm. Additionally, X-ray reflectivity (XRR, Bruker D8 diffractometer with Cu Kα radiation) was used to

cross-check the obtained film thickness values. The surface morphology was characterized with a Bruker Dimension Edge atomic force microscopy (AFM) system operated in tapping mode.

The chemical composition of the films was studied with X-ray photoelectron spectroscopy (XPS) and Fourier transform infrared spectroscopy (FTIR). XPS was performed on a Thermo Scientific Theta Probe tool with Al Kα radiation (15 kV, 70 W) on a 0.3 mm diameter spot focussed by a MXR1 monochromator. No depth profiling was performed as the Ar+ sputtering can cause inadvertent reduction of the Cu(II) species[35], as well as preferential removal of the elements. Instead, angle-resolved XPS was utilized to obtain further information on the depth distribution of the elements. As carbon is the main constituent of the samples, the typical charge referencing to adventitious C 1s peak could not be performed. However, we note that in all measured samples, the position of the oxygen impurity was constant at 531.5 eV. Therefore, we expect the observed changes in the peak positions between the samples to reflect the changes in the chemical composition of the films, and are not due to surface charging effects. The FTIR measurements were performed with a Bruker Model VERTEX 70V spectrometer with a DTGS detector. The measurements were performed in transmission mode on samples deposited on double-side polished Si(100) substrates. The spectrum of a blank Si wafer was used to subtract the background contribution of the substrate. The background was furthermore levelled to assist the comparison of the spectra. The UV-Vis-NIR spectra were collected with a Perkin Elmer Lambda 1050 UV-Vis-NIR spectrophotometer, using a spectralon-coated integrating sphere with PMT/InGaAs detectors to collect total transmission or reflection. For these measurements, Cu-DMD films of 15 nm thickness were deposited on quartz substrates. In case of the transmission spectra, the background of blank quartz substrate was subtracted from the measurement data. The reflection spectra include the contribution from the substrate.

For the electronic conductivity measurements the films were deposited on interdigitated electrode arrays (IDA) (Au, 5 µm electrode width, 5 µm gap). The annealing experiments were carried out in a home-built heating chamber under flowing H_2/He mixture (0.5 ml/min, 5% H2, supplied by Air Liquide), or under flowing O_2 (0.5 ml/min, 99.999 %, Air Liquide). The sample conductance was monitored with an Autolab PGSTAT702 potentiostat at set time intervals by conducting a voltage sweep in range of -0.5 V – 0.5V starting from 0 V. The temperature dependence of electrical resistance of the Cu-DMD thin films in high-conductance state was measured using a physical property measurement system (PPMS; Quantum Design), in a two-terminal current biased configuration. The excitation current was kept at 1µA. The conductance of the as-deposited samples was below the measurement limit of this setup. The conductivity (σ) of Cu-DMD was estimated from the measured conductance, G, values with $\sigma = (Gd)/(hlf)$, where d is the distance between the interdigitated electrodes, h is the Cu-DMD layer thickness, f is the number of IDA fingers, and l is their length.[36]

Grazing Incidence Wide Angle X-ray Scattering (GIWAXS) experiments were performed at NCD-SWEET beamline of the ALBA synchrotron light source (Spain). A X-ray beam of 12.4 keV (0.998 Å) or 16 keV (0.775 Å) for the *ex situ* and *in situ* samples respectively was prepared by using a Si (1 1 1) channel cut monochromator and further collimated with an array of Be lenses, obtaining a beam size at the sample position of 70 × 150 μm^2 (V × H). The 2D scattering patterns were recorded using a Rayonix LX255-HS area detector, which consists of an array of 5760 × 2880 (V × H) pixels with a pixel size of 88.54 × 88.54 μm^2 (V × H) for the employed binning of 2 × 2. An incident angle of 0.15° was employed. The scattering vector (q) was calibrated by using Cr_2O_3 as calibration standard.

Ex situ samples were measured in air using a sample holder placed on the rotation point of the available Huber stages, which allow precise x-y-z and tilt movements. Similarly, *in situ* experiments were performed by placing the sample on a heating stage inside a dedicated stainless-steel chamber, which was equipped with entrance and exit Kapton windows, a pump and a Mass Flow Controller system for gas injection. Samples were annealed at 170 °C during 2 h under a continuous flow of H_2 5% in He atmosphere (500 sccm, 1 bar). Data treatment (e.g. calibration, background subtraction, flat field and solid angle corrections) and reduction were done by combining PyFAI[37] with *in house* developed Python routine.

Computational details:

We studied Cu-DMD with Density Functional Theory (DFT), using the PBE0 hybrid density functional method (DFT-PBE0).[38,39] All-electron, Gaussian-type triple-ζ-valence + polarization (TZVP) basis sets derived from molecular Karlsruhe def2 basis sets were utilized.[40-43] All quantum chemical calculations were carried out using the CRYSTAL17 program package.[44] Spin polarization was taken into account in all calculations due to the open-shell nature of Cu(II) ions (magnetic configurations are given together with the coordinate listings in the Supporting Information). We compared both antiferromagnetic (AFM) and ferromagnetic ordering for the magnetic Cu(II) centres in Cu-DMD. The antiferromagnetic configuration is energetically favored by about 60 kJ/mol per Cu atom. AFM configuration was used also for the magnetic Cu(II) centres in the partially reduced Cu-DMD models (reduced Cu(I) centres are not magnetic).

For the evaluation of the Coulomb and exchange integrals (TOLINTEG), tight tolerance factors of 8, 8, 8, 8, and 16 were used. In geometry optimizations, both the atomic positions and lattice constants were fully optimized. All optimized structural models are given in CIF format in the Supporting Information. Default optimization convergence thresholds and DFT integration grids of CRYSTAL17 were applied.

For three-dimensional Cu-DMD systems, the reciprocal space was sampled using a 4×2×1 Monkhorst-Pack-type *k*-point mesh (*c*-axis was over 22 Å).[45] Fermi smearing of 0.005 a.u. (1600 K) was applied in the case of Cu-DMD reduced with two H_2 molecules per eight Cu-DMD units. The reciprocal space paths for the electronic band structures were obtained from the SeeK-path service.[46-48]

Calculating the IR spectra for the 3D structural models of Cu-DMD was not computationally feasible and the spectra were simulated for a one-dimensional chain with four Cu-DMD units. Two *k*-points were used to sample the reciprocal space in this case. The harmonic vibrational frequencies and IR intensities were obtained by using the computational schemes implemented in CRYSTAL.[49-51] The IR spectrum was obtained by using Lorenzian peak profile and FWHM of 8 cm^{-1}.

Result and discussion:

The N,N'-dimethyl dithiooxamidato copper (Cu-DMD) thin films were deposited using bis(dimethylamino-2-propoxy)copper(II) ($Cu(dmap)_2$) and N,N'-dimethyl-dithiooxamide as the precursors. $Cu(dmap)_2$ has previously been demonstrated beneficial for low temperature ALD/MLD processes,[52] whereas dithiooxamides are thus far unexplored.

The deposition process was monitored *in situ* with spectroscopic ellipsometry (SE) which shows well controlled, linear thickness increase with increasing number of deposition cycles after an initial regime of enhanced growth. (Figure 1b) The growth-per-cycle (GPC) shows saturative behaviour with precursor pulse lengths above 20 s for $Cu(dmap)_2$ and 35 s for DMD (Figure S1 in the Supporting Information). X-ray photoelectron spectroscopy (XPS) confirms the presence of C, S, N, and Cu in the as-deposited films with a nominal ratio of $CuC_{4.1}S_{2.3}N_{1.8}$, in good agreement with the expected composition of $CuC_4S_2N_2$ (Figure S2). Additionally, a small impurity (1.8 at-%) of oxygen is seen, that appears to be located mainly on the near surface region as determined by angle resolved XPS. Fourier-transform infrared (FTIR) measurements shown in Figure S3 confirm the formation of the target coordination polymer, with good agreement to the previously reported IR spectrum of Cu-DMD.[53] The as-deposited films are extremely smooth (RMS roughness of 0.27 nm) and uniform when examined with AFM. (Figure S4 a, b) In comparison, the RMS roughness of the bare Si substrate is measured to be 0.1 nm. X-ray reflectivity (XRR) measurements further confirm the long-range uniformity of the thin films. An exemplary XRR fit is shown in Figure S5.

Typically, dithiooxamide-based coordination polymers are amorphous or poorly crystalline.[54] Here, X-ray diffraction (XRD) measurements reveal the presence of a single prominent diffraction peak corresponding to d-spacing of 8.2 Å (Figure 1c). A detailed study on the films using grazing incidence wide angle X-ray scattering (GIWAXS) measurements reveal that the scattering intensity of the Bragg reflection is concentrated along the q_z axis indicating strong out-of-plane orientation. (Figure 1d) No

peaks arising from potential impurity phases are detected. It is further revealed that the ordering and preferred orientation are dependent on the substrate. With a TiN coated Si-substrate, the scattering intensity becomes more spread out. On a Pt coated substrate, the ordering effect is significantly weaker. (Figure S6a, b) Correspondingly, AFM images of the Cu-DMD on Pt show a larger grain size with much increased surface roughness. (Figure S4, e, f)

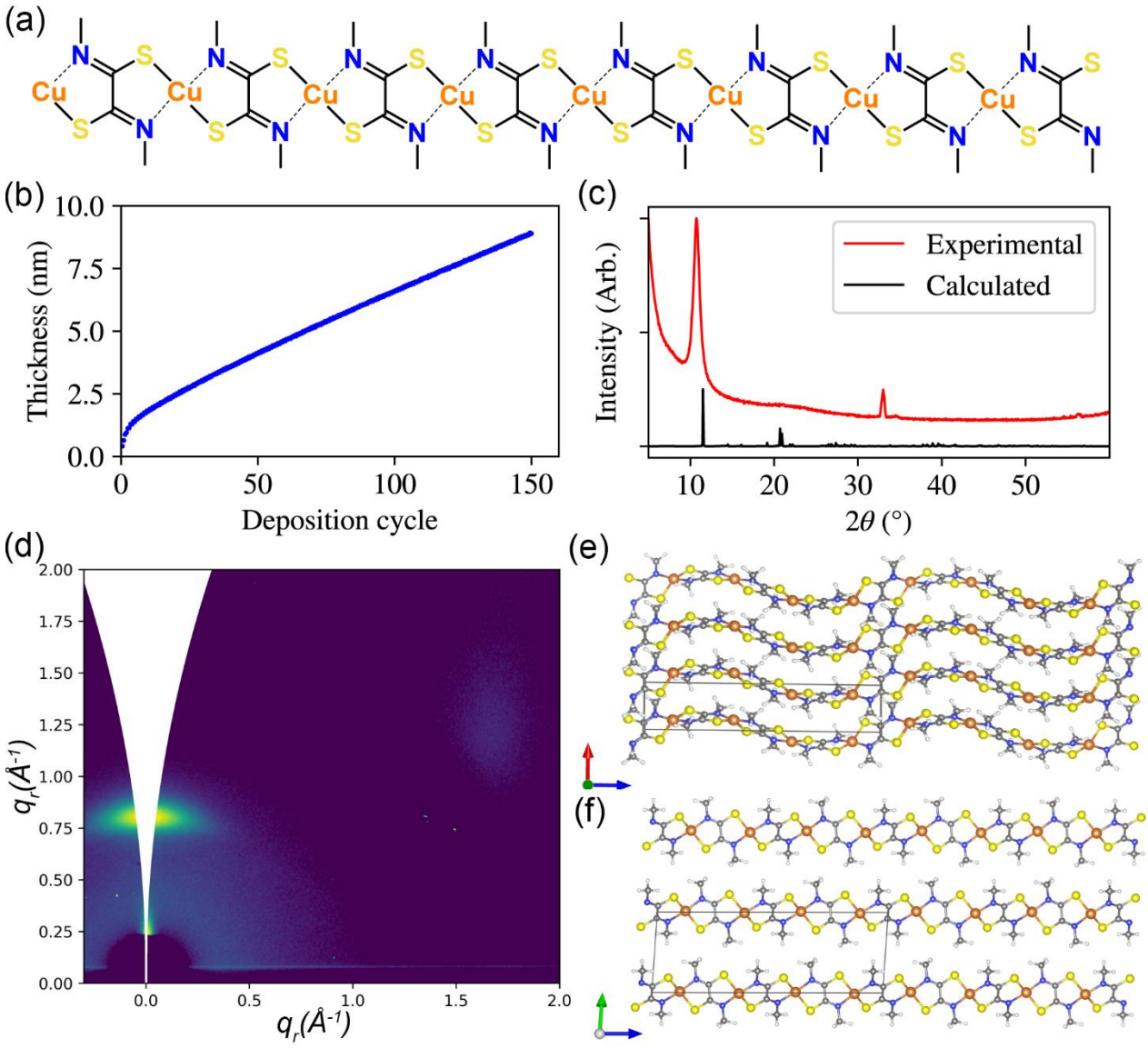

Figure 1. (a) Schematic of the Cu-DMD polymer chain, (b) Evolution of the Cu-DMD layer thickness as function of the deposition cycles monitored with *in situ* ellipsometry (c) The experimental (red) and theoretical (black) X-ray diffraction patterns of Cu-DMD. The peak at 33° in the experimental data originates from the Si substrate. (d) The corresponding GIWAXS plot showing strong out-of-plane orientation of the Cu-DMD thin films on Si with native oxide, (e) Geometry-optimized structure of the Cu-DMD thin films along the (100) plane and (f) along the (010) plane.

To fully understand the ordering and the orientation of the thin films, we used density functional theory (DFT) calculations to predict the thin film structure (DFT-PBE0/TZVP level of theory, see Computational Details in Supporting information). While a definite crystal structure for Cu-DMD is lacking in literature, two different motifs have been put forward: one with 1D copper dithiooxamide chains running parallel to each other,[54] and another with 2D planes with the copper sites assuming a paddlewheel configuration.[55] Of these, the 1D structure is common among other metal-dithiolene systems, and therefore considered the likely structure here. In our DFT-model, the polymeric chains are formed by sequential bridging of the metal centres with the DMD ligand in its *trans*-isomer (Figure 1a). The magnetic ordering of the metal centres is antiferromagnetic (at 0 K). The parallel alignment of the 1D chains then further results in a sheet-like secondary structure with the methyl groups separating adjacent sheets. (Figure 1e, f) The coordination mode of the Cu centres deviates from the typical square planar geometry of metal-dithiolenes. Tetrahedral distortion is induced by the nitrogen substitution as was hypothesized by Abboudi *et al*.[54] The distortion leads to 1D-chains with a helical shape (Figure 1e). The calculated diffraction pattern displays a prominent peak at d = 7.7 Å, arising from the stacking of the sheet-like secondary structure, in good agreement with the experimental pattern.(Figure 1b) Similar formation of a sheet-like secondary structure has been observed for 1D nickel-bis(dithiolene) coordination polymers.[56] It is likely that the static nature of the theoretical model exaggerates the ordering within the stacked layers. Thereby the absence of the other diffraction peaks in the experimental data is not unexpected. Further confirmation for the 1D-chain model is obtained from the theoretical infrared spectrum of the structure that also matches the experimental data (Figure S3).

Charge-carrier injection, or doping, via charge-transfer redox chemistry, or through electrochemical means is typically used to achieve high conductivity values in polymeric conductors.[57] Similarly, it is expected that the oxidation state of the coordination polymer is a major element in determining its conductivity.[12,58–61] Dithiooxamides belong to the group of redox-active dithiolene ligands, that are the backbone of many of the conducting coordination polymers. However, in comparison to other dithiolenes, the neutral dithiooxamide ligand is in the oxidized state and can undergo a two-electron reduction accompanied with protonation. The advantage of the present high-quality thin films is that they allow the *in situ* observation of conductance during the oxidation/reduction. For dithiooxamide-based coordination polymers, it has previously been observed that oxidative doping of these materials with I_2 or $FeCl_3$ can result in the increase of conductivity up to 5 orders of magnitude.[62,63] Also electrochemical reduction with concurrent proton incorporation has been used to tune the conductivity properties of various dithiooxamide based coordination polymers, although in these cases the changes in conductance have been ascribed to ionic conduction.[64] In the present work, we take advantage of

the catalytic activity of the open Cu(II) nodes of the polymer chains. Such sites are known to catalyse the H-H bond cleavage of molecular hydrogen.[65] In the case of the metal-organic framework $Cu_3(BTC)_2$, the hydrogen splitting leads to the protonation of the ligand, while the Cu node was reduced to metallic copper.[66] Here we speculate that with the redox-active ligands, the liberated electrons can instead delocalize over the polymer chain promoting electrical conductivity.

For the resistivity measurements, Cu-DMD films with thickness of 15 nm were deposited on interdigitated electrode arrays shown in Figure S7a. This approach limited us to 2-electrode measurements only, but was necessary given the low overall conductance of the samples. As deposited, the samples initially display a low conductivity of $< 10^{-10}$ S/cm at room temperature, with linear dependence of $\log(\sigma)$ vs $T^{-1/4}$, indicative of a variable-range hopping type conduction. (Figure S8 a,b). As shown in Figure 2a, when the samples were heated in 5% H_2/He atmosphere at 170 °C, the conductivity increased significantly during the annealing process, ultimately stabilizing at around $3x10^{-3}$ S cm^{-1}. Linear I-V relationship was observed before and after the hydrogen treatment, indicative of ohmic behaviour. (Figure S7b). However, during the experiment at around the 40 min mark, the I-V response momentarily deviated from purely ohmic as illustrated in Figure S7 c and d, resulting in the observed jump in Figure 2a. After the annealing, the high conducting state was retained upon cooling and interestingly, upon subsequent exposure to ambient air, the conductivity initially increases further up to 10^{-2} S/cm, yielding an overall increase of ca. 8 orders of magnitude. (Figure S9a) This could be related to partial reoxidation of the film upon air exposure and could hint of a conduction maximum at a distinct oxidation state. The observed conductivity value of the H_2-treated CuDMD films was additionally verified using an alternative four-electrode geometry (Figure S10a). AC conductivity measurements indicate almost purely capacitive behaviour for the samples in the low-conductivity state, whereas purely resistive behaviour is observed for the high-conductivity state. (Figures S10b and c, respectively) Long term storage in ambient air results in slow decay of the conductivity over several weeks. Heat treatment under flowing O_2 at up to 130 °C decreased the conductivity to 10^{-9} S cm^{-1}.(Figure S9b)

The temperature dependency of electrical resistivity in the high-conductance state is shown in Figure 2b. Remarkably, it shows metallic behaviour down to 2 K. Above 20 K and up to 300 K, the resistance increases linearly with increasing temperature, whereas below 20 K the slope flattens out and becomes independent of temperature. As with the *in situ* measurements, short term air exposure resulted in increase in the conductance, whereas storage in ambient conditions for 2 months decreases the electrical conductance about one order of magnitude. The metal-like temperature dependency of electrical resistivity was systematically observed at these stages of air exposure. (Figure S11)

We used various techniques to gain further insight into the H_2-reduction induced conductance change. *In situ* GIWAXS measurements recorded during the annealing show that the primary diffraction peak of Cu-DMD gradually shifts to slightly lower d-value indicating a decrease in the lattice dimension. (Figure 2c) No significant change in the preferred orientation is seen. It is also apparent that no new crystalline phases are formed during the annealing. (Figure S12).

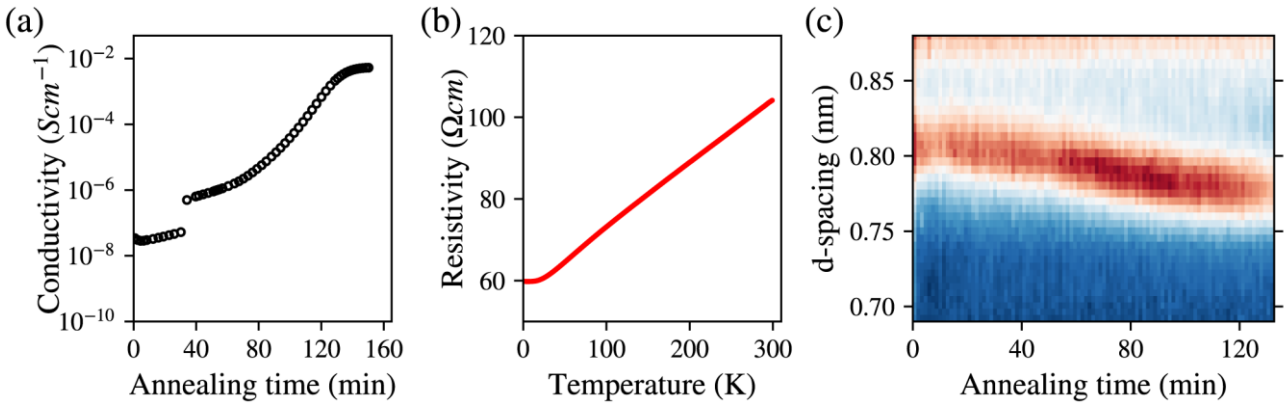

Figure 2. (a) the evolution of the Cu-DMD conductance during the annealing in H_2/He atmosphere at 170 °C. (b) Temperature dependency of Cu-DMD resistance in the high-conducting state. (c) *in situ* GIWAXS data during the annealing process showing the shift of the diffraction peak towards lower d-value.

The XPS spectra of Cu 2p, N 1s, S 2p, and C 1s core level peaks recorded at various stages of H_2-annealing are shown in Figures S13 – S16. In the Cu 2p spectra of the as deposited sample, alongside with the main Cu $2p_{3/2}$ and $2p_{1/2}$ lines, prominent satellite peaks are present at the high energy side of the main lines that are typical for Cu^{2+} compounds. It is also clear that the $2p_{3/2}$ and $2p_{1/2}$ peaks consist of two components (deconvolution of $2p_{3/2}$ shown in Fig. S13), with the second component on the low energy side corresponding to Cu^{1+}. Based on the oxidation state of the $Cu(dmap)_2$ precursor, only Cu^{2+} would be expected. The mixed-valence state may reflect the redistribution of the electron density arising from the mixing of the metal and ligand orbitals.[67] With increasing annealing time in H_2/He, it is apparent that the proportion of Cu^{1+} increases, indicating that reduction of the thin films is induced by the H_2-treatment. Similar change in the Cu oxidation state was observed for bulk N,N'-bis-(hydroxyethyl) substituted dithiooxamidato-copper complexes upon electrochemical reduction.[68] The N 1s spectra (Figure S14) show an appearance of a second component as a shoulder on the high-energy side of the main line upon prolonged H_2-treatment. This may reflect the conversion of the nitrogen bonding environment from imine-type nitrogen to amine-type due to protonation of the ligand.[69] In the S 2p spectra (Figure S15), the main observation is the small shift towards higher energy as the

annealing time increases. All the spectra can be fitted with a single set of $2p_{3/2}$ - $2p_{1/2}$ doublet, although noteworthy is that the FWHM values increase from 1.05 eV of the as deposited spectrum to 1.25 eV for the sample annealed for 3 h. This might indicate the presence of a secondary sulphur environment overlapping the primary one. In the C 1s spectra (Figure S16), no major changes are apparent.

In the FTIR spectra, a new absorption band emerges in the region typical for amine N-H stretching mode (Figure S17) after the H_2-treatment. Otherwise, the FTIR spectrum remains relatively unchanged with only shifts in intensity, while peak positions remain constant. AFM measurements taken after annealing reveal that the surface remains smooth and uniform with a slight reduction in the surface roughness. (Figure S4 c,d) The film thickness remained constant for timescales considered in Fig. 2, but more prolonged annealing lead to decrease in thickness that might be related to partial decomposition of the films after certain degree of reduction. UV-Vis-NIR spectra taken in transmission mode for the as-deposited sample, and after annealing are shown in Figure S18a. The transmittance minimum for the as deposited film is located at 379 nm. In addition, a shoulder extending to 1000 nm is observed. Upon annealing in H_2/He, these features are diminished, but there is decrease in the transmission from 1000 nm to 2500 nm. Reflectance measurements (Figure S18b) indicate that this feature can be fully ascribed to increased reflectance of the annealed film in this region.

Therefore, it is evident that the increase in the conductance is intrinsic to the main Cu-DMD phase and not due to formation of a secondary conductive phase such as CuS or metallic copper. It appears that the Cu-DMD film is capable of catalysing the hydrogen molecule splitting, whereupon the Cu-DMD film is partly reduced. Given the conjugated system, the additional electrons would result in increase of charge carrier density, whereas the protons are localized to the nitrogen atoms in the form of secondary amines.

To further elucidate the effect of the H_2 treatment on the Cu-DMD thin films, we used the previously constructed theoretical structural model to conduct first principles calculations on the effect of protonation on the electronic structure. In this model we assumed that the hydrogen molecules are adsorbed to the open Cu sites followed by homolytic cleavage of the H-H bond as illustrated in Figure S19. Here we studied models with 1 and 2 hydrogen molecules per 8 Cu sites to reflect the apparent degree of protonation of our samples as estimated from the amine-to-imine peak area ratio of the XPS N1s spectra. In accordance to the experimental findings, the lowest energy structure was found upon formation of amine groups on the adjacent ligands of the catalytic copper site. By observing the change of partial charge at the Cu nodes, we can deduce that the main Cu site is reduced from Cu^{2+} to Cu^{1+}. Delocalization over the ligand is also apparent with partial reduction of the adjacent Cu site. Electronic band structures for the pristine and reduced Cu-DMD are shown in Figures 3 a, b, and c. For the pristine material, a wide band gap of 3.2 eV is estimated with nearly flat energy bands that reflect the

molecular nature of the compound. As such, the electronic structure is consistent with the observed low conductance of the as deposited samples, as well as with the measured UV-Vis-NIR spectrum. Partial reduction with one hydrogen molecule (i.e. 2 protons, 2 electrons) added per 8 Cu sites, leads to the formation of a new in-gap dispersive band that intersects the Fermi level along the Γ–X direction. This corresponds to the *a*-axis of the unit cell, indicating interchain interaction between neighbouring chains within the 2D sheet-like secondary structure. With further reduction we can see a further appearance of in-gap bands with increased bandwidth. Alongside the changes in electronic structure, we can observe structural changes withing the 2D-secondary structure. (1) The aforementioned cleavage of Cu-N bonds to form secondary amines, and (2) the interchain Cu-S interactions become stronger as the amount of H atoms increases (Fig. S20). We should point out that the model considered here is quite idealistic with perfectly aligned polymer chains and reduction sites, whereas the real case is likely more random. For the reduced Cu-DMD the low bandwidths of the in-gap bands are consistent with the observed moderate conductance of 10^{-2} Scm^{-1}. A higher conductance might be achievable by substituting the amine group with a thiol group. Indeed, in case of nickel-ethylenetetrathiol (Ni-ett), theoretical calculations predict the formation of a similar half-filled, metallic band upon oxidation, with a significantly higher bandwidth.[70]

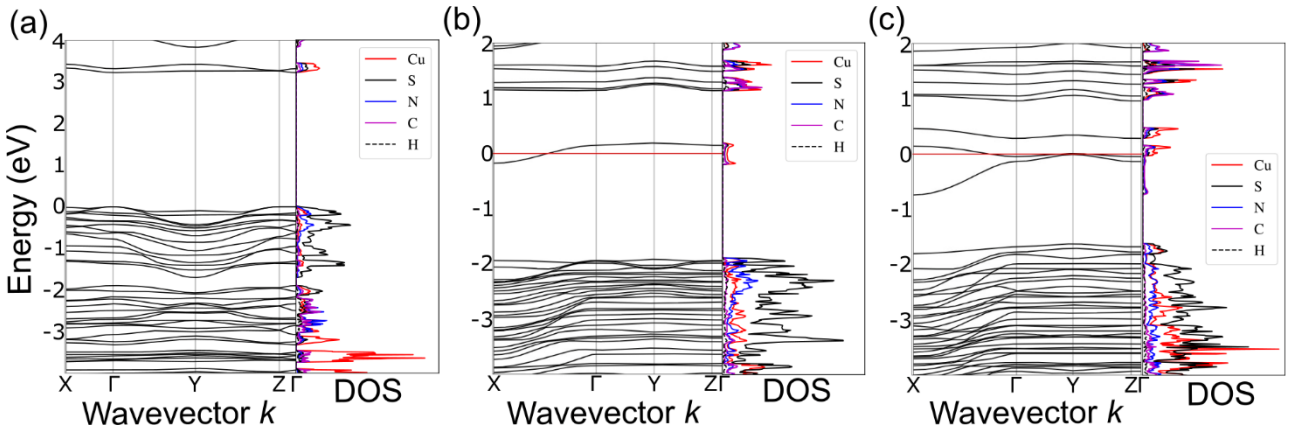

Figure 3. Calculated band structures and density-of-states plots of the Cu-DMD model at various degrees of reduction: (a) pristine, (b) $2H^+/2e^-$ per 8 Cu, and (c) $4H^+/4e^-$ per 8 Cu. The plots are shown for one spin channel (spin-up). In (b) and (c), the Fermi level is indicated with the red line.

Conclusions:

We have demonstrated the fabrication of high-quality 1D coordination polymer thin films of N,N-dimethyldithiooxamidato copper by ALD/MLD. We find that the electrical conductivity of the films can be adjusted over 8 orders of magnitude from initial 10^{-10} S cm^{-1} up to 10^{-2} S cm^{-1} by reductive doping induced by mild thermal treatment in H_2 containing atmosphere. Temperature dependent

electrical conductivity measurements reveal a semiconductor-to-metal transition upon the reductive doping. Metallic behaviour of electrical conductivity is observed in the temperature range of 2 – 300 K. DFT calculations point to the formation of a half-filled conduction band that arises from the increased interchain interaction and the formation of extended (-Cu-S-)$_n$ conduction pathways. It seems that the good agreement between the theoretical and experimental findings arise from the high degree of orientation in the thin films. Therefore, the ALD/MLD approach could be a beneficial synthesis approach for other conductive coordination polymers such as the 2D-nanosheets. Furthermore, the influence of the redox state on the conductivity is clearly demonstrated and opens up the possibility for nanodevices with tuneable conductance.

Author Information Notes:

Corresponding authors: Mikko Nisula (mikko.nisula@ugent.be), Christophe Detaverner (christophe.detavernier@ugent.be)

Supporting Information:

Supplementary figures S1 – S20 (Includes ALD/MLD growth characteristics, XPS data, FTIR spectra, AFM images, XRR data, additional GIWAXS data, additional electrical characterization, UV-Vis-NIR spectra, additional structural images), Structure models for the pristine and reduced Cu-DMD optimized at the DFT-PBE0/TZVP level of theory in CIF format.

Acknowledgements:

This project has received funding from the European Union's Horizon 2020 research and innovation programme under the Marie Skłodowska-Curie grant agreement No 841995. Synchrotron X-ray scattering experiments were performed at NCD-SWEET beamline at ALBA synchrotron with the collaboration of ALBA staff (project number 2019023379). J. Dendooven, J.-Y. Feng, M. Filez and R. K. Ramachandran are acknowledged for assisting with the *in situ* GIWAXS experiments. A J. K. would like to thank Mr. Kim Eklund for helpful computational analyses on one-dimensional Cu-DMD models, Academy of Finland for funding (grant no. 317273), and CSC - the Finnish IT Center for Science for computing resources. H.S.J. acknowledges FWO [PEGASUS]2 Marie Sklodowska-Curie grant agreement no. 665501 for Incoming postdoctoral fellowship.

References:

(1) Deng, X.; Hu, J. Y.; Luo, J.; Liao, W. M.; He, J. Conductive Metal–Organic Frameworks:

Mechanisms, Design Strategies and Recent Advances. *Top. Curr. Chem.* **2020**, *378*, 27. https://doi.org/10.1007/s41061-020-0289-5.

(2) Givaja, G.; Amo-Ochoa, P.; Gomez-Garcia, C. J.; Zamora, F. Electrical Conductive Coordination Polymers. *Chem. Soc. Rev.* **2012**, *41* (1), 115–147. https://doi.org/10.1039/c1cs15092h.

(3) Stassen, I.; Burtch, N.; Talin, A.; Falcaro, P.; Allendorf, M.; Ameloot, R. An Updated Roadmap for the Integration of Metal-Organic Frameworks with Electronic Devices and Chemical Sensors. *Chem. Soc. Rev.* **2017**, *46* (11), 3185–3241. https://doi.org/10.1039/c7cs00122c.

(4) Gómez-Herrero, J.; Zamora, F. Coordination Polymers for Nanoelectronics. *Adv. Mater.* **2011**, *23* (44), 5311–5317. https://doi.org/10.1002/adma.201101952.

(5) Huang, X.; Sheng, P.; Tu, Z.; Zhang, F.; Wang, J.; Geng, H.; Zou, Y.; Di, C. A.; Yi, Y.; Sun, Y.; Xu, W.; Zhu, D. A Two-Dimensional π-d Conjugated Coordination Polymer with Extremely High Electrical Conductivity and Ambipolar Transport Behaviour. *Nat. Commun.* **2015**, *6*, 7408. https://doi.org/10.1038/ncomms8408.

(6) Darago, L. E.; Aubrey, M. L.; Yu, C. J.; Gonzalez, M. I.; Long, J. R. Electronic Conductivity, Ferrimagnetic Ordering, and Reductive Insertion Mediated by Organic Mixed-Valence in a Ferric Semiquinoid Metal-Organic Framework. *J. Am. Chem. Soc.* **2015**, *137* (50), 15703–15711. https://doi.org/10.1021/jacs.5b10385.

(7) DeGayner, J. A.; Jeon, I. R.; Sun, L.; Dincă, M.; Harris, T. D. 2D Conductive Iron-Quinoid Magnets Ordering up to Tc = 105 K via Heterogenous Redox Chemistry. *J. Am. Chem. Soc.* **2017**, *139* (11), 4175–4184. https://doi.org/10.1021/jacs.7b00705.

(8) Clough, A. J.; Orchanian, N. M.; Skelton, J. M.; Neer, A. J.; Howard, S. A.; Downes, C. A.; Piper, L. F. J.; Walsh, A.; Melot, B. C.; Marinescu, S. C. Room Temperature Metallic Conductivity in a Metal-Organic Framework Induced by Oxidation. *J. Am. Chem. Soc.* **2019**, *141* (41), 16323–16330. https://doi.org/10.1021/jacs.9b06898.

(9) Dong, R.; Han, P.; Arora, H.; Ballabio, M.; Karakus, M.; Zhang, Z.; Shekhar, C.; Adler, P.; Petkov, P. S.; Erbe, A.; Mannsfeld, S. C. B.; Felser, C.; Heine, T.; Bonn, M.; Feng, X.; Cánovas, E. High-Mobility Band-like Charge Transport in a Semiconducting Two-Dimensional Metal–Organic Framework. *Nat. Mater.* **2018**, *17* (11), 1027–1032. https://doi.org/10.1038/s41563-018-0189-z.

(10) Gao, J.; Geng, S.; Chen, Y.; Cheng, P.; Zhang, Z. Theoretical Exploration and Electronic

Applications of Conductive Two-Dimensional Metal–Organic Frameworks. *Top. Curr. Chem.* **2020**, *378*, 25. https://doi.org/10.1007/s41061-020-0288-6.

(11) Chen, S.; Dai, J.; Zeng, X. C. Metal-Organic Kagome Lattices M3(2,3,6,7,10,11-Hexaiminotriphenylene)2 (M = Ni and Cu): From Semiconducting to Metallic by Metal Substitution. *Phys. Chem. Chem. Phys.* **2015**, *17* (8), 5954–5958. https://doi.org/10.1039/c4cp05328a.

(12) Kambe, T.; Sakamoto, R.; Kusamoto, T.; Pal, T.; Fukui, N.; Hoshiko, K.; Shimojima, T.; Wang, Z.; Hirahara, T.; Ishizaka, K.; Hasegawa, S.; Liu, F.; Nishihara, H. Redox Control and High Conductivity of Nickel Bis(Dithiolene) Complex π-Nanosheet: A Potential Organic Two-Dimensional Topological Insulator. *J. Am. Chem. Soc.* **2014**, *136* (41), 14357–14360. https://doi.org/10.1021/ja507619d.

(13) Dou, J. H.; Sun, L.; Ge, Y.; Li, W.; Hendon, C. H.; Li, J.; Gul, S.; Yano, J.; Stach, E. A.; Dincă, M.; Gul, S. Signature of Metallic Behavior in the Metal-Organic Signature of Metallic Behavior in the Metal-Organic Frame- Works M 3 (Hexaiminobenzene) 2 (M = Ni , Cu). *J. Am. Chem. Soc.* **2017**, *139*, 13608−13611. https://doi.org/10.1021/jacs.7b07234.

(14) Clough, A. J.; Skelton, J. M.; Downes, C. A.; De La Rosa, A. A.; Yoo, J. W.; Walsh, A.; Melot, B. C.; Marinescu, S. C. Metallic Conductivity in a Two-Dimensional Cobalt Dithiolene Metal-Organic Framework. *J. Am. Chem. Soc.* **2017**, *139* (31), 10863–10867. https://doi.org/10.1021/jacs.7b05742.

(15) Huang, X.; Zhang, S.; Liu, L.; Yu, L.; Chen, G.; Xu, W.; Zhu, D. Superconductivity in a Copper(II)-Based Coordination Polymer with Perfect Kagome Structure. *Angew. Chemie - Int. Ed.* **2018**, *57* (1), 146–150. https://doi.org/10.1002/anie.201707568.

(16) Kitagawa, H.; Onodera, N.; Ahn, J. S.; Mitani, T.; Toriumi, K.; Yamashita, M. The Metallic State in a MMX-Chain Complex, Pt2(Dta)4I. *Synth. Met.* **1997**, *86* (1–3), 1931–1932. https://doi.org/10.1016/s0379-6779(97)80968-x.

(17) Kitagawa, H.; Onodera, N.; Sonoyama, T.; Yamamoto, M.; Fukawa, T.; Mitani, T.; Seto, M.; Maeda, Y. Charge Ordering with Lattice Distortions in a Conductive MMX-Chain Complex, Pt2(Dta)4I (Dta = CH3CS2-). *J. Am. Chem. Soc.* **1999**, *121* (43), 10068–10080. https://doi.org/10.1021/ja9915910.

(18) Calzolari, A.; Alexandre, S. S.; Zamora, F.; Di Felice, R. Metallicity in Individual MMX Chains. *J. Am. Chem. Soc.* **2008**, *130* (16), 5552–5562. https://doi.org/10.1021/ja800358c.

(19) Welte, L.; Calzolari, A.; Di Felice, R.; Zamora, F.; Gómez-Herrero, J. Highly Conductive Self-Assembled Nanoribbons of Coordination Polymers. *Nat. Nanotechnol.* **2010**, *5* (2), 110–115. https://doi.org/10.1038/nnano.2009.354.

(20) Campbell, M. G.; Powers, D. C.; Raynaud, J.; Graham, M. J.; Xie, P.; Lee, E.; Ritter, T. Synthesis and Structure of Solution-Stable One-Dimensional Palladium Wires. *Nat. Chem.* **2011**, *3* (12), 949–953. https://doi.org/10.1038/nchem.1197.

(21) Shi, W.; Wu, G.; Hippalgaonkar, K.; Wang, J. S.; Xu, J.; Yang, S. W. Poly(Nickel-Ethylenetetrathiolate) and Its Analogs: Theoretical Prediction of High-Performance Doping-Free Thermoelectric Polymers. *J. Am. Chem. Soc.* **2018**, *140* (41), 13200–13204. https://doi.org/10.1021/jacs.8b08270.

(22) Reynolds, J. R.; Jolly, C. A.; Krichene, S.; Cassoux, P.; Faulmann, C. Poly (Metal Tetrathiooxalates): A Structural and Charge-Transport Study. *Synth. Met.* **1989**, *31* (1), 109–126. https://doi.org/10.1016/0379-6779(89)90631-0.

(23) Castillo-Blas, C.; Montoro, C.; Platero-Prats, A. E.; Ares, P.; Amo-Ochoa, P.; Conesa, J.; Zamora, F. The Role of Defects in the Properties of Functional Coordination Polymers. In *Advances in Inorganic Chemistry*; Elsevier Inc., 2020; Vol. 76, pp 73–119. https://doi.org/10.1016/bs.adioch.2020.03.002.

(24) Foster, M. E.; Sohlberg, K.; Allendorf, M. D.; Talin, A. A. Unraveling the Semiconducting/Metallic Discrepancy in Ni3(HITP)2. *J. Phys. Chem. Lett.* **2018**, *9* (3), 481–486. https://doi.org/10.1021/acs.jpclett.7b03140.

(25) Day, R. W.; Bediako, D. K.; Rezaee, M.; Parent, L. R.; Skorupskii, G.; Arguilla, M. Q.; Hendon, C. H.; Stassen, I.; Gianneschi, N. C.; Kim, P.; Dincă, M. Single Crystals of Electrically Conductive Two-Dimensional Metal-Organic Frameworks: Structural and Electrical Transport Properties. *ACS Cent. Sci.* **2019**, *5* (12), 1959–1964. https://doi.org/10.1021/acscentsci.9b01006.

(26) Sundberg, P.; Karppinen, M. Organic and Inorganic–Organic Thin Film Structures by Molecular Layer Deposition: A Review. *Beilstein J. Nanotechnol.* **2014**, *5*, 1104–1136. https://doi.org/10.3762/bjnano.5.123.

(27) Stassen, I.; De Vos, D.; Ameloot, R. Vapor-Phase Deposition and Modification of Metal-Organic Frameworks: State-of-the-Art and Future Directions. *Chem. - A Eur. J.* **2016**, *22* (41), 14452–14460. https://doi.org/10.1002/chem.201601921.

(28) Solomos, M. A.; Claire, F. J.; Kempa, T. J. 2D Molecular Crystal Lattices: Advances in Their Synthesis, Characterization, and Application. *J. Mater. Chem. A* **2019**, *7* (41), 23537–23562. https://doi.org/10.1039/c9ta06534b.

(29) Nisula, M.; Linnera, J.; Karttunen, A. J.; Karppinen, M. Lithium Aryloxide Thin Films with Guest-Induced Structural Transformation by ALD/MLD. *Chem. - A Eur. J.* **2017**, *23* (13), 2988–2992. https://doi.org/10.1002/chem.201605816.

(30) Ahvenniemi, E.; Karppinen, M. In-Situ Atomic/Molecular Layer-by-Layer Deposition of Inorganic-Organic Coordination Network Thin Films from Gaseous Precursors. *Chem. Mater.* **2016**, *28* (17), 6260–6265. https://doi.org/10.1021/acs.chemmater.6b02496.

(31) Penttinen, J.; Nisula, M.; Karppinen, M. Atomic/Molecular Layer Deposition of s-Block Metal Carboxylate Coordination Network Thin Films. *Chem. - A Eur. J.* **2017**. https://doi.org/10.1002/chem.201703704.

(32) Tanskanen, A.; Karppinen, M. Iron-Terephthalate Coordination Network Thin Films Through In-Situ Atomic/Molecular Layer Deposition. *Sci. Rep.* **2018**, *8* (1), 1–8. https://doi.org/10.1038/s41598-018-27124-7.

(33) Khayyami, A.; Philip, A.; Karppinen, M. Atomic/Molecular Layer Deposited Iron–Azobenzene Framework Thin Films for Stimuli-Induced Gas Molecule Capture/Release. *Angew. Chemie* **2019**, *131* (38), 13534–13538. https://doi.org/10.1002/ange.201908164.

(34) Woodburn, H. M.; Sroog, C. E. The reaction of cyanogen with organic compounds. V. Mercaptans, *J. Org. Chem.* **1952**, *17*, 371–378. https://doi.org/10.1021/jo01137a007

(35) Panzner, G.; Egert, B.; Schmidt, H. P. The stability of CuO and Cu_2O during argon sputtering studied by XPS and AES *Surf. Sci.* **1985,** *151,* 400–408. https://doi.org/10.1016/0039-6028(85)90383-8

(36) Karlsson, C.; Suga, T.; Nishide, H. Quantifying TEMPO Redox Polymer Charge Transport toward the Organic Radical Battery *Appl. Mater. Interfaces* **2017**, *9*, 10692–10698. https://doi.org/10.1021/acsami.7b00403

(37) Ashiotis, G.; Deschildre, A.; Nawaz, Z.; Wright, J. P.; Karkoulis, D.; Picca F. E.; Kieffer, J. The fast azimuthal integration Python library: pyFAI *J. Appl. Cryst*. **2015**, *48*, 510–519. https://doi.org/10.1107/S1600576715004306

(38) Perdew, J. P.; Burke, K.; Ernzerhof, M. Generalized Gradient Approximation Made Simple, *Phys. Rev. Lett.* **1996**, *77*, 3865. https://doi.org/10.1103/PhysRevLett.77.3865

(39) Adamo, C.; Barone, V. Toward Reliable Density Functional methods without Adjustable Parameters: The PBE0 Model. *J. Chem. Phys.* **1999**, *110*, 6158. https://doi.org/10.1063/1.478522

(40) Weigend, F.; Ahlrichs, R. Balanced Basis Sets of Split Valence, Triple Zeta Valence and Quadruple Zeta Valence Quality for H to Rn: Design and Assessment of Accuracy. *Phys. Chem. Chem. Phys*. **2005**, *7*, 3297−305. https://doi.org/10.1039/B508541A

(41) Ab initio study on lattice thermal conductivity of Cu_2O using GGA and hybrid density functional methods Linnera, J.; Karttunen, A. J. *Phys. Rev. B* **2017**, *96*, 014304. http://doi.org/10.1103/PhysRevB.96.014304

(42) Glebko, N.; Aleksandrova I.; Tewari, G. C.; Tripathi, T. S.; Karppinen, M.; Karttunen, A. J. Electronic and Vibrational Properties of TiS_2, ZrS_2, and HfS_2: Periodic Trends Studied by Dispersion-Corrected Hybrid Density Functional Methods, *J. Phys. Chem. C*, **2018**, *122*, 26835–26844. http://doi.org/10.1021/acs.jpcc.8b08099

(43) Karttunen, A. J.; Tynell, T.; Karppinen, M. Layer-by-Layer Design of Nanostructured Thermoelectrics: First-Principles Study of ZnO:Organic Superlattices Fabricated by ALD/MLD, *Nano Energy* **2016**, *22*, 338–348. http://doi.org/10.1016/j.nanoen.2016.02.028

(44) Dovesi, R, Erba, A, Orlando, R, et al. Quantum-mechanical condensed matter simulations with CRYSTAL. *WIREs Comput Mol Sci*. 2018; 8:e1360. https://doi.org/10.1002/wcms.1360

(45) Monkhorst, H. J.; Pack, J. D. Special Points for Brillouin-Zone integrations. *Phys. Rev. B* **1976**, *13*, 5188−5192. https://doi.org/10.1103/PhysRevB.13.5188

(46) Hinuma,Y.; Pizzi, G.; Kumagai, Y.; Oba, F.; Tanaka, I. Band structure diagram paths based on crystallography, *Comp. Mater. Sci*. **2017**, *128*, 140. https://doi.org/10.1016/j.commatsci.2016.10.015

(47) Togo, A.; Tanaka, I.; Spglib: a software library for crystal symmetry search (2018). https://arxiv.org/abs/1808.01590

(48) https://www.materialscloud.org/work/tools/seekpath.

(49) Pascale, F.; Zicovich-Wilson, C. M.; Gejo, F. L.; Civalleri, B.; Orlando, R.; Dovesi, R. The calculation of the Vibrational Frequencies of Crystalline Compounds and its Implementation in the CRYSTAL Code. *J. Comput. Chem*. **2004**, 25, 888−897. https://doi.org/10.1002/jcc.20019

(50) Zicovich-Wilson, C. M.; Pascale, F.; Roetti, C.; Saunders, V. R.; Orlando, R.; Dovesi, R. Calculation of the Vibration Frequencies Of Alpha-Quartz: the Effect of Hamiltonian and Basis Set. *J. Comput. Chem*. **2004**, *25*, 1873−1881. https://doi.org/10.1002/jcc.20120

(51) Maschio, L.; Kirtman, B.; Orlando, R.; Rèrat, M. Ab initio analytical infrared intensities for periodic systems through a coupled perturbed Hartree-Fock/Kohn-Sham method *J. Chem. Phys.* **2012**, 137, 204113. https://doi.org/10.1063/1.4767438

(52) Hagen, D. J.; Mai, L.; Devi, A.; Sainio, J.; Karppinen, M. Atomic/Molecular Layer Deposition of Cu-Organic Thin Films. *Dalt. Trans.* **2018**, *47* (44), 15791–15800. https://doi.org/10.1039/C8DT03735C.

(53) Desseyn, H. O.; Jacob, W. A.; Herman, M. A. Infra-Red Absorption Spectra of Complexes of Dithio-Oxamides. *Spectrochim. Acta* **1969**, *25A*, 1685–1692. https://doi.org/10.1016/0584-8539(69)80156-X.

(54) Abboudi, M.; Mosset, A.; Galy, J. Metal Complexes of Rubeanic Acid. 3.1 Large-Angle X-Ray Scattering Studies of Amorphous Copper(II) and Nickel(II) Complexes. *Inorg. Chem.* **1985**, *24* (13), 2091–2094. https://doi.org/10.1021/ic00207a026.

(55) Kanda, S.; Ito, K.; Nogaito, T. Magnetic and Electrical Properties of Coordination Polymers Formed with Copper and Rubeanic Acid. *J. Polym. Sci. Part C Polym. Symp.* **1967**, *17*, 151–162. https://doi.org/10.1002/polc.5070170112.

(56) Matsuoka, R.; Sakamoto, R.; Kambe, T.; Takada, K.; Kusamoto, T.; Nishihara, H. Ordered Alignment of a One-Dimensional π-Conjugated Nickel Bis(Dithiolene) Complex Polymer Produced via Interfacial Reactions. *Chem. Commun.* **2014**, *50* (60), 8137–8139. https://doi.org/10.1039/c4cc02022g.

(57) Wegner, G. Polymers with Metal-Like Conductivity—A Review of Their Synthesis, Structure and Properties. *Angew. Chemie Int. Ed. English* **1981**, *20* (4), 361–381. https://doi.org/10.1002/anie.198103611.

(58) Kambe, T.; Sakamoto, R.; Hoshiko, K.; Takada, K.; Miyachi, M.; Ryu, J. H.; Sasaki, S.; Kim, J.; Nakazato, K.; Takata, M.; Nishihara, H. π-Conjugated Nickel Bis(Dithiolene) Complex Nanosheet. *J. Am. Chem. Soc.* **2013**, *135* (7), 2462–2465. https://doi.org/10.1021/ja312380b.

(59) Aubrey, M. L.; Wiers, B. M.; Andrews, S. C.; Sakurai, T.; Reyes-Lillo, S. E.; Hamed, S. M.; Yu, C. J.; Darago, L. E.; Mason, J. A.; Baeg, J. O.; Grandjean, F.; Long, G. J.; Seki, S.; Neaton, J. B.; Yang, P.; Long, J. R. Electron Delocalization and Charge Mobility as a Function of

Reduction in a Metal-Organic Framework. *Nat. Mater.* **2018**, *17* (7), 625–632. https://doi.org/10.1038/s41563-018-0098-1.

(60) Jiang, Y.; Oh, I.; Joo, S. H.; Buyukcakir, O.; Chen, X.; Lee, S. H.; Huang, M.; Seong, W. K.; Kwak, S. K.; Yoo, J. W.; Ruoff, R. S. Partial Oxidation-Induced Electrical Conductivity and Paramagnetism in a Ni(II) Tetraaza[14]Annulene-Linked Metal Organic Framework. *J. Am. Chem. Soc.* **2019**, *141* (42), 16884–16893. https://doi.org/10.1021/jacs.9b08601.

(61) Wentz, H. C.; Skorupskii, G.; Bonfim, A. B.; Mancuso, J. L.; Hendon, C. H.; Oriel, E. H.; Sazama, G. T.; Campbell, M. G. Switchable Electrical Conductivity in a Three-Dimensional Metal-Organic Framework: Via Reversible Ligand n-Doping. *Chem. Sci.* **2020**, *11* (5), 1342–1346. https://doi.org/10.1039/c9sc06150a.

(62) Nagels, P.; Mertens, R.; Desseyn, H. O. Electrical Properties of Cu (II) -N , N H -Dimethyldithiooxamide Polymers. *Synth. Met.* **2002**, *128*, 1–6. https://doi.org/10.1016/S0379-6779(01)00545-8.

(63) Vallejo-Sánchez, D.; Amo-Ochoa, P.; Beobide, G.; Castillo, O.; Fröba, M.; Hoffmann, F.; Luque, A.; Ocón, P.; Pérez-Yáñez, S. Chemically Resistant, Shapeable, and Conducting Metal-Organic Gels and Aerogels Built from Dithiooxamidato Ligand. *Adv. Funct. Mater.* **2017**, *27* (15). https://doi.org/10.1002/adfm.201605448.

(64) Nagao, Y.; Ikeda, R.; Kanda, S.; Kubozono, Y.; Kitagawa, H. Complex-Plane Impedance Study on a Hydrogen-Doped Copper Coordination Polymer: N,N′-Bis-(2-Hydroxyethyl)Dithiooxamidato-Copper(II). *Mol. Cryst. Liq. Cryst.* **2002**, *379*, 89–94. https://doi.org/10.1080/713738672.

(65) Halpern, J. Homogeneous Catalytic Activation of Molecular Hydrogen by Metal Ions and Complexes. *J. Phys. Chem.* **1959**, *63* (3), 398–403. https://doi.org/10.1021/j150573a015.

(66) Grzech, A.; Yang, J.; Dingemans, T. J.; Srinivasan, S.; Magusin, P. C. M. M.; Mulder, F. M. Irreversible High-Temperature Hydrogen Interaction with the Metal Organic Framework Cu3(BTC)2. *J. Phys. Chem. C* **2011**, *115* (43), 21521–21525. https://doi.org/10.1021/jp206821f.

(67) Ivanova, T. M.; Maslakov, K. I.; Sidorov, A. A.; Kiskin, M. A.; Linko, R. V.; Savilov, S. V.; Lunin, V. V.; Eremenko, I. L. XPS Detection of Unusual Cu(II) to Cu(I) Transition on the Surface of Complexes with Redox-Active Ligands. *J. Electron Spectros. Relat. Phenomena* **2020**, *238*, 146878. https://doi.org/10.1016/j.elspec.2019.06.010.

(68) Fujishima, M.; Ikeda, R.; Kanda, S.; Kitagawa, H. Electronic State of a Hydrogen-Doped Copper Coordination Polymer: N,N′-Bis-(Hydroxyethyl)Dithiooxamidatocopper(II), (HOC 2H4)2dtoaCu. *Mol. Cryst. Liq. Cryst.* **2002**, *379*, 223–228. https://doi.org/10.1080/713738609.

(69) Wang, C. Y.; Gray, J. L.; Gong, Q.; Zhao, Y.; Li, J.; Klontzas, E.; Psofogiannakis, G.; Froudakis, G.; Lueking, A. D. Hydrogen Storage with Spectroscopic Identification of Chemisorption Sites in Cu-TDPAT via Spillover from a Pt/Activated Carbon Catalyst. *J. Phys. Chem. C* **2014**, *118* (46), 26750–26763. https://doi.org/10.1021/jp507395p.

(70) Liu, Y.; Shi, W.; Zhao, T.; Wang, D.; Shuai, Z. Boosting the Seebeck Coefficient for Organic Coordination Polymers: Role of Doping-Induced Polaron Band Formation. *J. Phys. Chem. Lett.* **2019**, *10* (10), 2493–2499. https://doi.org/10.1021/acs.jpclett.9b00716.

For table of contents graphics only: